Correlative Extinction and Single Fluorophore Bleaching Microscopy for Ligand Quantification on Gold Nanoparticles

Nicole Slesiona, Lukas Payne, Iestyn Pope, Paola Borri, Wolfgang Langbein, and Peter Watson*

Nanoparticles (NPs) are promising therapeutic delivery agents, with the number and manner of presentation of cell-binding ligands on the NP affecting the eventual fate of the therapeutic. Whenever NPs are conjugated with biomolecules, a heterogeneous population of decorated NPs will be produced and these subpopulations of particle-ligand structures need to be characterized for a reliable interpretation of NP-based data. An optical microscopy method is reported to quantitatively evaluate the conjugation on a single-particle basis in samples consisting of gold NPs (GNPs) decorated with holo-transferrin fluorescently labeled with Alexa647 (Tf). Widefield fluorescence and extinction microscopy are employed on NP-ligand constructs, alongside a correlative analysis that spatially co-localizes diffraction-limited sources of fluorescence with the optical extinction by individual GNPs. A photobleaching step analysis estimates the number of fluorophores contributing to the detected emission rate. The method quantifies the number of fluorescent biomolecules attached per GNP, the numbers of unconjugated GNPs and unbound Tf present within the mixed population, and the size and intraparticle clustering propensity of conjugated GNPs. A high variability is found in the number of Tf ligands per GNP within the GNP population, when analyzed at the single-particle level, unraveling a non-trivial statistical distribution not accessible in ensemble-averaged approaches.

1. Introduction

Metal nanoparticles (MNPs) have generated ever-increasing attention as they have become an integral part in catalysis,[1–3]

N. Slesiona, L. Payne, I. Pope, P. Borri, P. Watson
School of Biosciences
Cardiff University
Museum Avenue, Cardiff CF10 3AX, UK
E-mail: WatsonPD@cardiff.ac.uk

L. Payne, W. Langbein
School of Physics and Astronomy
Cardiff University
The Parade, Cardiff CF24 3AA, UK

The ORCID identification number(s) for the author(s) of this article can be found under https://doi.org/10.1002/admi.202300568

biomedical detection,[4–6] nano-therapy,[7–9] and as imaging labels.[10–13] Of specific interest are gold nanoparticles (GNPs) due to their low cytotoxicity, high biocompatibility, chemical stability, and their unique optical properties in the visible range of light that depend on their size and shape.[14,15] Their surface chemistry and geometrical characteristics can either enhance or hamper their specificity and reliability for the intended application.[16,17] Both properties can be controlled as GNPs can be synthesized in a variety of sizes and shapes with a narrow size distribution in a single-phase reaction. Biofunctionalization of GNPs is a crucial step in the creation of nanocarriers with targeted sensory and/or therapeutic relevance and requires careful consideration of the involved reagents to ensure colloidal stability at a range of pH levels and salt concentrations of their surrounding medium. Generally, GNPs are coated with bi-functional polymers such as polyethylene glycol (PEG) to stabilize them against aggregation and to introduce chemical moieties for their subsequent biofunctionalization. The surface density of the stabilizing capping agent will govern their stability and half-life in the body, while the nature and density of targeting molecules (TMs) control specific binding. The density of the latter may control the uptake mechanisms induced by the nanocarrier, as this property–in conjunction with the GNP shape, level of curvature, and size–influences the way TMs are presented to an analyte or a biological membrane.

Both GNP size and TM surface density need thorough evaluation to allow the correct interpretation of GNP-based data, facilitate their use as imaging agents, and to allow them to transition into clinical applications. Generally, current quantification methods on MNPs begin with the determination of the total particle surface area by gas adsorption analysis[18,19] or by measuring the average MNP size of the ensemble by dynamic light scattering (DLS),[20,21] transmission electron microscopy (TEM),[22–24] or scanning electron microscopy (SEM).[23] Subsequently, the total number of TMs in the sample is determined. Quantitative methods include thermogravimetric analysis (TGA),[24,25] optical spectroscopy,[26] detaching the TMs from the particle
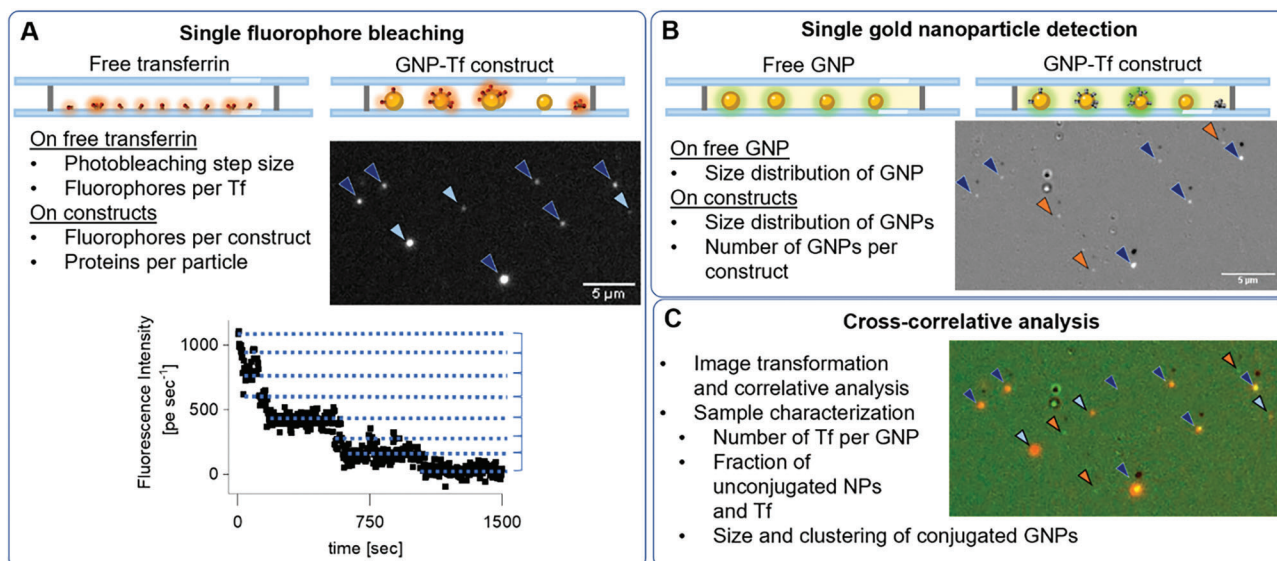
Figure 1. Methodology of correlative measurements of single fluorophore bleaching and extinction microscopy. NP constructs consist of spherical GNPs decorated with fluorescently labeled human holo-transferrin (Tf). A) The fluorescence intensity of individual free Tf, as well as of GNP-Tf constructs, spin-coated onto a glass surface is imaged by widefield microscopy over time until all fluorophores are bleached. The bleaching step size per fluorophore and in turn the number of fluorophores per protein is determined. The fluorescence intensity of GNP-Tf constructs is then used to quantify the number of Tf contributing to an individual GNP. Fluorescence spots (not) co-occurring with extinction spots are marked with dark blue (light blue) arrows. B) The extinction cross-sections of particles in the area that was previously photobleached are quantified using widefield extinction microscopy. The number of GNPs contributing to an individual spot can be estimated from the average extinction cross-section of individual particles. Extinction spots (not) co-localized with a fluorescence spot are marked with a dark blue (orange) arrow. C) Fluorescence and extinction images are overlaid using a transformation that accounts for shift, scaling, rotation, and shear between images acquired in different microscopes, to allow evaluation for co-localization of fluorescence and extinction spots.

and measuring their concentration in solution,[27,28] by nuclear magnetic resonance (NMR)[24,29] or vibrational spectroscopy.[30] Emerging techniques such as pH-based methods, electrospray-differential mobility analysis, and X-ray photoelectron spectroscopy (XPS) also show promising results for the field of TM quantification.[24,31] The average particle size and the total number of TMs in the sample are then used to calculate the average TM surface density on an average-sized MNP in the ensemble. Knowing this average density may be sufficient to judge whether a conjugation reaction has been successful, however further information on the heterogeneity of the population is needed to correctly interpret experiments. Functionalization reactions of NPs with TMs inevitably produce a polydisperse sample. Apart from unconjugated NPs and unconjugated TMs, the sample can contain NPs with varying biomolecule number and spatial distribution, aggregates of NPs cross-linked by the TMs, as well as TM aggregates. Indeed, there have been studies revealing missing colocalization between NPs and fluorescent TMs thought to be attached on the NP surface.[32,33] This polydispersity makes interpretation of cell uptake with TM functionalized NPs challenging. For example, pure TM aggregates will generate a fluorescence signal that could be interpreted as a NP bound to the cell membrane, whilst cross-linked NPs may reach a size too large to be internalized by mammalian cells.[16,34]

At present, there is no method to evaluate the parameters quantifying a sample's polydispersity of NP size and number of TMs binding to the NP on a particle-by-particle basis. For NPs, we are limited to ensemble quantification meth-

ods that evaluate the number of biomolecules per particle on average.[35]

In this work, we present a method that allows quantification of TM numbers on GNPs on a particle-by-particle basis. This is realized by a correlative analysis of fluorescence and extinction microscopy images of GNP constructs, here using functionalized spherical GNPs decorated with the fluorescently labeled ligand human holo-transferrin (Tf). Single-molecule bleaching data reveal the number of fluorophores contributing to the fluorescence of a single Tf, and in turn, quantify the number of Tfs per GNP (**Figure 1**A). Wide-field extinction microscopy allows the determination of the size and the estimated number of GNPs contributing to the extinction spots (Figure 1B). Extinction microscopy is a method to quantitatively measure extinction cross-sections of hundreds of MNPs simultaneously using commonly available optical components. Absolute extinction cross-section values are then retrieved by an automated analysis, which allows a high-throughput characterization of NP sizes.[36,37] An image transformation software is used to create matching fluorescence and extinction images of the same area to analyze the co-occurrence of extinction and fluorescence signals. The analysis produces a quantifiable output with respect to the number of attached Tf per GNP, the fraction of successfully functionalized GNPs versus unconjugated GNPs versus free Tf in a sample, and the number of GNPs that have been cross-linked by the reaction procedure (Figure 1C). The method is also capable of generating a measure for how many Tfs have been cross-linked without a GNP present in the aggregate. Notably, these aggregates might be misinterpreted as successfully

internalized particle-ligand constructs in fluorescence-based microscopy measurements. Our analysis can provide information to guide the optimization of the functionalization reaction using for example different concentrations of ligands, cross-linkers, and particles.

2. Experimental Section

2.1. Samples

2.1.1. GNP Functionalization with Tf

Three GNP-Tf constructs were utilized in this work, differing in their ratios of proteins to attachment sites on the GNP (see **Table 1**). Commercially available GNPs (Nanopartz Ntracker, Salt Lake City, UT) were used with 14 nm (sample 1) and 20 nm (samples 2 and 3) average diameter and a proprietary coating of stabilizing hydrophilic polymer with terminal amine groups (two attachment sites per nm^2 surface area, specified by the manufacturer). For conjugation with commercially available Alexa647-labeled human holo-transferrin (Tf, Thermo Fisher, Loughborough, Leicestershire, UK), sulfo-succinimidyl-4-(N-maleimidomethyl)-cyclohexane-1-carboxylate (sulfo-SMCC) was used. A schematic illustration of the functionalization reaction is available in Figure S1 (Supporting Information). Ratios of protein to available attachment sites on the GNPs were formulated as follows: 0.01 Tf per attachment site in sample 1, 0.4 Tf per attachment site in sample 2, and 1 Tf per attachment site in sample 3. This was realized by diluting the GNP concentration and keeping the concentration of Tf constant at 340 nM. First, the GNPs were conjugated to the NHS functional group of the cross-linker by adding a 100x excess of sulfo-SMCC to amine residues. The reaction was left on a shaker at room temperature for an hour after which the GNPs were purified by centrifugation at 12000 rcf for 20 min. The supernatant (≈90%) was removed and replaced with PBS (pH 7) containing 340 nM Tf. The reaction was left for 2 h at room temperature on a shaker while protecting the samples from light. After incubation, to remove unbound Tf the sample was purified by centrifugation at 12000 rcf for 20 min, 90% of the supernatant was removed and discarded, and the particles were resuspended to a volume of 1 mL 1% (v/v) PBS 0.01% (v/v) Tween 20 solution. The purification step was applied three times, and after the last step of supernatant removal, GNPs were resuspended to a final volume of 1 mL with PBS. Additionally, a control sample was assessed in which the functionalization reaction was conducted without the presence of GNP to check for protein cross-linking following the procedure. The functionalized GNPs were stored at 4 °C until usage for a maximum of 1 month.

Table 1. Gold nanoparticle-transferrin construct samples used in the experiments.

Sample	1	2	3
Mean particle diameter [nm]	14	20	20
Attachment sites per particle	1230	2500	2500
Ratio of attachment sites to Tfs	0.01	0.4	1

2.1.2. Sample Preparation for Imaging

A 24 × 24 mm (thickness 0.16–0.19 mm, Menzel–Gläser, #1.5, Braunschweig, Germany) H$_2$O$_2$-cleaned cover slip was placed on the chuck of a spin coater (WS-650MZ-23NPPB, Laurell, USA) and immobilized by vacuum. The disk was set to spin for 35 s at 2000 rpm followed by another 30 s at 4000 rpm. During the first 5 s of rotation, 20 µL of sample were pipetted onto the center of the spinning cover slip. Given that single Tfs and GNPs were smaller than the resolution achievable on diffraction-limited optical imaging systems, fluorescence signals from individual Tfs or GNP-Tf constructs appeared as spots with a size given by the point spread function (PSF) of the microscope. The size of the PSF was a function of the numerical aperture (NA) of the objective used, the illumination wavelength, and the refractive index of the surrounding medium. Where two nano-objects were much closer than the size of the PSF, they would not be separated and appear as a single object. To minimize the likelihood of such events, the Tf, the GNP, and the GNP-Tf constructs were diluted to a density of 10^9 mL^{-1} before spin-coating. Considering the 20 µL of sample used and a cover slip surface area of 576 mm^2 this corresponds to 0.035 particles µm^{-2} (average particle distance 5 µm) when assuming a uniform coating of the cover slip. Before spin-coating, a diamond scribe was used to create marks on the glass surface to allow measurements of the same area on different microscope platforms. The sample was then mounted onto a glass slide with the spin-coated surface toward the slide, using a 0.12 mm thick adhesive gasket (Grace Bio-lab SecureSeal) modified with channels to allow the injection of index matching oil for extinction microscopy.

2.2. Data Acquisition and Processing

2.2.1. Wide-Field Epi-Fluorescence Microscopy and Data Processing

Wide-field epi-fluorescence measurements were conducted on an inverted Olympus IX73 microscope and a Prior Lumen200Pro light source using filter set (89000, Chroma, Vermont, U.S.A.) selecting the ET645 nm/30 nm as the excitation filter and the ET705 nm/72 nm as the emission filter. A schematic illustration of the set-up is shown in Figure S2 (Supporting Information). The emission was detected with a scientific-CMOS (sCMOS) Camera (Hamamatsu ORCA-flash 4.0 V2, 30000 full well capacity, 1.4 electrons read noise, and 0.46 electrons per count) at a 2 × 2 binning readout on all images corresponding to a 130 nm image pixel size. Camera and filter settings were operated utilizing the HCImage software package (Hamamatsu). A 100× oil immersion objective with an adjustable NA of 0.6–1.3 was used. The objective NA was set to 0.95 to avoid total internal reflection that was found to create a significant background by residual transmission of the filters. An aperture iris was not available in the fly-eye illuminator of the IX73, which would have enabled limiting the NA of the illumination while collecting the emission with the highest NA for maximum signal. To determine the number of fluorophores per Tf and the number of Tf per GNP, spin-coated samples of Tf and GNP-Tf were measured in a time series with 3 s integration time. To obtain a reproducible excitation intensity, a red fluorescent slide (ThorLabs-FSK6), was mounted and

ADVANCED
SCIENCE NEWS

www.advancedsciencenews.com

ADVANCED
MATERIALS
INTERFACES
Open Access

www.advmatinterfaces.de

the lamp intensity was adjusted to achieve an average signal of 50 000 counts at 50 ms exposure time. To minimize photobleaching prior to measurement the sample was focused in bright field contrast at minimum light intensity without any filters in place. To remove background including hot pixels, a background image was acquired using an average of 20 frames with the same acquisition settings but without fluorescence excitation and subtracted from the time series. The data was evaluated using an image analysis software suite developed in-house (Extinction Suite Macro[37,38]) to extract the fluorescence intensity of an individual spot, spatially summed over the PSF, versus time to determine steps of photobleaching. For each fluorescent spot, the data was summed over a 4-pixel radius around its peak, and a local background from the surrounding data up to 8-pixels radius was subtracted. The suite assigns an index to each spot to allow cross-referencing to its corresponding extinction spot for co-occurrence analysis. Details of the analysis software and its calculations were discussed in Payne et al..[37] Steps of photobleaching were evaluated manually and the resulting distributions were plotted to quantify the average number of fluorophore ligands present per individual Tf, subsequently used to determine the number of Tf per GNP.

2.2.2. Wide-Field Extinction Microscopy

Following photobleaching measurements, the chamber of the sample was filled with silicone oil, index matched to glass (n = 1.52), to reduce background caused by surface roughness in extinction measurements. Extinction microscopy was performed as described by Payne et al..[36] Briefly, measurements were performed on a Nikon Ti-U inverted microscope, using a 100 × 1.45 NA oil objective (Nikon lambda series, MRD01905) with a 1× tube lens, and a 1.34NA condenser. The sample was illuminated by a halogen tungsten lamp (V2-A LL 100 W; Nikon) with a bandpass filter in the illumination path of 550 ± 20 nm (Thorlabs FB500-40). A schematic illustration of the set-up is shown in Figure S2 (Supporting Information). Extinction images were obtained with a sCMOS camera (PCO Edge 5.5), with 2560×2160 pixels and 16-bit digitization, 0.54 electrons per count, and a full well capacity of 30 000 electrons. The exposure time was set to 12 ms for each frame, using an 82 Hz frame rate and an average signal of $\approx 22\,000$ photoelectrons (pe). To acquire a differential transmission image, the area of interest was imaged twice with the particles in focus, with a lateral sample shift of 1.3 µm. Background images were acquired by blocking the illumination path. To achieve the required sensitivity in extinction cross-section, 1280 frames were acquired for each of the shifted positions. To reduce the effect of slow drifts in illumination and sensor, only 128 frames were sequentially acquired at fixed sample position, and the position was cycled ten times. The resulting σ_{ext} data had a noise of ≈ 15 nm.^{2} An extinction image was calculated using the averages of all frames at each respective position as described in Payne et al.[36] and was conducted with the same analysis software that was used for fluorescence intensity evaluation. Also, here an index was assigned to each spot detected by the software for cross-referencing to their corresponding fluorescence spot. To estimate the particle size from the extinction cross-section σ_{ext}, MiePlot v4.6.18 was used to simulate σ_{ext} for

GNPs in oil (n = 1.52) averaged over the wavelengths 535, 545, 555, and 565 nm according to the illumination wavelength range selected by the bandpass filter. Notably, this simulation used the gold dielectric function of Johnson & Christy,[39] which did not take into account the surface scattering in small particles.[40] This can result in an overestimation of the absorption cross-section by ≈ 10–30%, in turn leading to an underestimation of the particle size by 3–10% considering the scaling of σ_{ext} with the particle volume in the investigated small size regime.

2.3. Correlative Image Analysis

All images were evaluated using ImageJ. Because extinction and bleaching measurements of the same areas were acquired on different microscope systems, extinction images were transformed into the fluorescence images to correct for scaling, shear, rotation, and translation differences, using an in-house written image transformation software. Based on a number N of common features identified by their coordinates of fluorescence ($\mathbf{r}_f$) and extinction ($\mathbf{r}_e$) signals, the software determines a transformation

$$\mathbf{r}_f = C\mathbf{r}_e + \mathbf{t} \tag{1}$$

where $\mathbf{t}$ is a translation vector, and the matrix C rotates, shears, and scales the axes. The transformation parameters are determined by minimizing the standard deviation S between $\mathbf{r}_f$ and the transformed $\mathbf{r}_e$, given by

$$S = \sqrt{\frac{1}{N} \sum \left| \mathbf{r}_f - \left(C\mathbf{r}_e + \mathbf{t} \right) \right|^2} \tag{2}$$

At the minimum of N = 3 required, the transformation is exact, so that S = 0. The transformed image that can be overlapped with its reference image for correlation analysis (Figure 1C). Details of the registration method are described in Pope et al.[10] Overlapped images were evaluated manually to assess co-localization of extinction and fluorescence signals.

3. Results and Discussion

3.1. Determination of Fluorophore Bleaching Step Size

Free Tf and GNP-Tf construct samples were imaged on a wide-field microscope in epifluorescence to measure the fluorescence rate over time for the evaluation of the mean bleaching step size I_B. Its value allows us to calculate the number N_F of fluorophores per Tf (or GNP-Tf construct), by dividing the fluorescence rate $I(t_0)$ detected for an individual spot in the image at the initial time point t_0 in the sequence, by I_B, so that

$$N_F = \frac{I(t_0)}{I_B} \tag{3}$$

I_B was determined for fluorophores attached to free Tf (number of analyzed spots N = 91) and GNP-Tf constructs (N = 95), see Figure S3 (Supporting Information). Free Tf showed a mean I_B of 150 ± 79 pe s^{-1}, and GNP-Tf a mean I_B of 142 ± 48 pe s.$^{-1}$ Combined populations give a mean I_B of 146 pe s^{-1}, which we
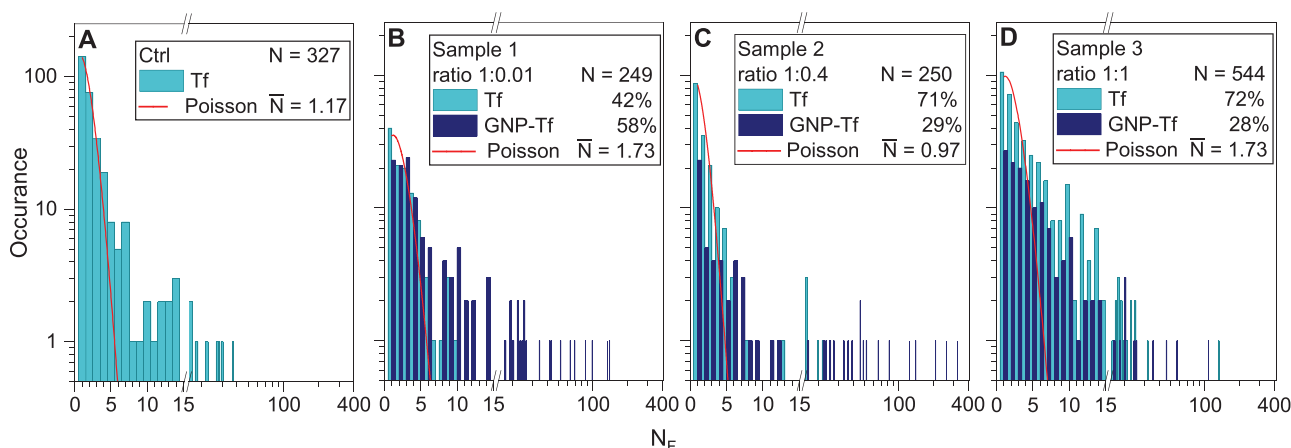
Figure 2. Distributions of fluorophore numbers on free Tf and GNP-Tf constructs. A) Distribution of N_F for free Tf (light blue) and GNP-Tf constructs (dark blue) on a sample containing free Tf, and on GNP-Tf B) Sample 1, C) Sample 2, and D) Sample 3. Fractions of GNP-Tf represent fluorescent particles only, i.e., do not include non-fluorescent particles. Data show initial fluorescence rates from time course experiments in epifluorescence mode (from the first frame with 3 s integration time). The Poisson fit to the distribution of the non-conjugated proteins is represented in red.

use in the following. Fluorophores have been shown to have a distribution of bleaching step sizes.[41] Plasmonic NP is known to alter fluorescence intensity depending on the distance of the fluorophore to the NP.[42] Fluorophore quenching has been shown to affect a fluorophore to a distance of up to 15 nm for GNP of 10 nm diameter with a steep decrease in its effects the larger the distance between fluorophore and GNP.[43] The GNPs utilized in our experiments come with a proprietary polymer corona to stabilize them against aggregation in cellular environments for in vitro applications, that may prevent or reduce fluorophore quenching due to the GNP. The exact nature of this polymer is not disclosed by the vendor but general in vitro studies of GNP make use of PEGylation at molecular weights of 500–5000 kDa, resulting in a polymer thickness of 4–16 nm.[44,45] In addition to the polymer thickness, the transferrin in Tf may act as a spacer between the polymer coating and the fluorophore, adding up to 4 nm distance[46] depending on how Tf attaches to the polymer and the location of the fluorophore on transferrin. The resulting total distance of 8–20 nm from the GNP may limit the effect of quenching on the detected rates. Additionally, excitation rates are also affected and in general, enhanced in the vicinity of GNPs due to an enhanced local electric field. Thus, while it is somewhat surprising that the observed bleaching step sizes are similar for free Tf and GNP Tf, it is possible within our mechanistic understanding.

3.2. Determination of Number of Fluorophores per Tf and Number of Tfs per GNP

As stated in the previous section, we determine the number of fluorophores N_F by dividing the fluorescence rate (fluorescence intensity spatially integrated over the PSF area of an individual spot in the image) with the photobleaching step size. **Figure 2**A shows the histogram of fluorescence rates on a sample containing only free Tf. To calculate N_F we use the average photobleaching step size of 146 pe s^{-1} per fluorophore, and the histogram binning is centered at these step sizes. Transferrin conjugated to

a single fluorophore shows the highest occurrence, and it should be noted that transferrin conjugated to zero fluorophores is not detected. The average number of fluorophores per protein $\bar{N}$ was determined by fitting the data to a Poisson distribution yielding $\bar{N} = 1.17$ (see Figure 2; Figure S4, Supporting Information, for further statistics). The manufacturer specification states a labeling rate of between 1 and 3 fluorophores per transferrin, with the ensemble measurement for this lot given as 2. Our particle analysis demonstrates that while the ensemble average tends to 2, the majority of visible structures contain only a single fluorophore, as indicated by the Poisson distribution. Panels B-D of Figure 2 show the histogram of N_F from the fluorescence of samples 1 to 3 respectively, with the values originating from Tf not colocalized with a GNP shown in light blue and GNP-Tf constructs in dark blue. Samples 1 and 2 (Figure 2B,C) show a wide distribution of fluorescence rates from GNP-Tf constructs. In both cases, the ratios of attachment site to ligand of 1:0.01 and 1:0.4 during functionalization do not fully saturate the available reaction sites and therefore increase the probability of two GNPs conjugating to the same Tf. This is supported by the larger fraction of constructs with a fluorescence rate corresponding to more than 15 fluorophores, 15% in sample 1 and 26% in sample 2, compared to 7% in sample 3. The difference between samples 1 and 2 relates to their different sizes of GNPs (14 and 20 nm), providing approximately twice the surface area and thus ligand attachment sites in sample 2. The small fraction of 7% in sample 3 indicates suppressed cross-linking of GNPs. Additionally, a control sample was assessed in which the functionalization reaction was conducted without the presence of GNP to check for protein cross-linking following the procedure. The distributions of unconjugated Tf yield a $\bar{N}$ of 1.73 in sample 1, 0.98 in sample 2, and 1.73 in sample 3 according to the Poisson distributions. This change in the population of remaining free Tf could be explained by either a) a low level of cross-linking between the proteins, or b) predominant binding of single fluorophore-conjugated protein to GNPs, removing these proteins from the free-Tf pool remaining. The change in population profile of free Tf following conjugation is sample-specific and so also provides information

**ADVANCED
SCIENCE NEWS**

www.advancedsciencenews.com

**ADVANCED
MATERIALS
INTERFACES**

www.advmatinterfaces.de

on the end products of the functionalization reaction. A control sample in which the functionalization reaction was conducted without the presence of GNPs did not return any fluorescence signal. This is in contrast to reactions containing GNPs where free transferrin aggregates, not associated with a GNP, can be observed. This indicates that Tf-aggregates do not purify in the absence of GNPs, and are associated loosely/non-covalently to the corona of the particles during centrifugation/purification. Cross-linking between the proteins is possible assuming that a portion of sulfo-SMCC is not removed by the intermediate purification step between particle activation and Tf addition. Sulfo-SMCC is a heterobifunctional reagent that is frequently used for cross-linking proteins with an *N*-hydroxylsuccinimide polyethylene (NHS) end on one side of the reagent and a maleimide group on the other. The NHS ester can form stable amide bonds with the primary amine groups on the GNP. In a pH range of 6.5–7.5 the maleimide moiety reacts with sulfhydryls in the protein but loses specificity at pH >7.5 which is why the pH should be closely monitored during reactions.[47] This opens the possibility for any remaining unconjugated bifunctional cross-linkers to attach to primary amines in the protein chain on one end, and to thiols on the other. It should be noted that the GNP construct samples used for these experiments were purified by centrifugation, the common method for MNP purification after functionalization with biomolecules.[48] The fraction of fluorescence not colocalized with GNPs is high in all samples (42%, 71%, and 72%) despite purification. This might have serious implications for the evaluation of fluorescence microscopy-based data sets, as signals visible in fluorescence microscopy images would originate from free or aggregated proteins while nominally being attributed to GNP constructs. It is unclear if these free proteins derive from insufficient purification or if they detached over time after the functionalization reaction.

3.3. Determination of Particle Size Distribution and Cross-Linking of Particles

We have shown in our previous work[32] that the size of MNPs can be determined quantitatively by measuring the extinction cross-section σ_{ext} of individual NPs. We have applied this method here on the same GNP-Tf construct samples imaged by wide-field fluorescence to verify the presence and size of individual GNPs. Moreover, we determined the number of particles N_{NP} contributing to an extinction signal, in the case of NP multimers (dimers, trimers, etc.) within the PSF, from the ratio between the measured σ_{ext} and the average cross-section value of a single particle σ_{sp}.

$$N_{NP} = \frac{\sigma_{ext}}{\sigma_{sp}} \tag{4}$$

The expected extinction cross-sections of GNPs of 14 and 20 nm diameter can be calculated as described in Section 2.2.2 to be of 179 and 547 nm^2 respectively. The measured σ_{ext} of individual GNPs has a mean value of 156 ± 85 nm^2 in sample 1, and 566 ± 374 nm^2 in the other samples, consistent with the nominal diameter from the manufacturer. It should be noted that at a constant volume but varying aspect ratios, σ_{ext} can vary by

up to 20% for aspect ratios between 0.8 and 1.2, which would have an impact of up to 7% on the size evaluation in extinction microscopy.[36] Larger aspect ratios could even cause them to be evaluated as dimers or multimers. For this reason, the particle morphologies of both batches were measured in TEM. Figure S5 (Supporting Information) shows no strongly non-spherical particles in the batch that was used for sample 1 (N = 305), and only a small fraction (4%) of such particles in the batch used for samples 2 and 3 (N = 297) (Figure S5G–I, Supporting Information). Therefore, signals originating from dimers and multimers can be linked to the functionalization procedure rather than oddly shaped particles. **Figure 3** shows the histograms of N_{NP} measured on the GNP-Tf construct samples (Figure 3B–D) and on a control sample using unconjugated 20 nm GNPs prior to functionalization (Figure 3A). The results have been separated into GNPs without (GNP, orange) and with (GNP-Tf, dark blue) fluorescence by the correlative fluorescence-extinction analysis described in Section 2.3. We find that 28% to 64% of GNPs in all construct samples have no fluorescence (Figure 3B–D) despite the excess of protein to attachment site and amount of unconjugated protein still present in the sample (see Figure 2B–D, and summarised in **Figure 4**D). A possible reason could be due to the bonds formed by sulfo-SMCC being not stable and shifted toward dissociation with every step of purification. Another mechanism could be that free Tf forms a protein corona around the constructs that is bound strong enough to stay associated with the construct (soft corona[49,50]) during purification by centrifugation, but not during spin coating when samples are prepared for imaging due to the strong shear flow. There is a similar variability in the distribution of multimer particles ($N_{NP} > 1$) in samples 1 and 2 (Figure 3B,C) with significantly less multimers in sample 3 (Figure 3D), consistent with the previous suggestion of inter-particle cross-linking depending on the ratio of ligands to attachment sites on the particles. In sample 3, the fraction of unfunctionalized particles is lower (28%) compared to samples 1 and 2 (53% and 64%, respectively) suggesting a higher functionalization probability with higher excess of Tf to GNP, as generally recommended in functionalization protocols of the cross-linkers. Lastly, fluorophore degradation without loss of protein could impact the fraction of unconjugated GNP reported. This might either happen during sample preparation or while finding focus in low-light conditions during the bleaching experiments. It should, therefore, be noted that this analysis represents a conservative evaluation of the ligand density on GNP in which the density might be under-but generally not overestimated.

3.4. Correlation of Fluorescence and Extinction Signals

More information on the functionalization beyond the histograms shown can be extracted from the correlative analysis of fluorescence and extinction signals (see Experimental Section 2.3), by evaluating the extinction cross-sections against fluorescence rates on a single particle basis, as shown in Figure 4A–C. From this correlation, it can be noted that sample 1 (Figure 4A), which used the smallest ratio of Tf to GNP, shows a cluster of σ_{ext} in the 100–400 nm^2 range with fluorescence rates in the 100–1000 pe s^{-1} range. Additionally, at higher extinction and fluorescence values, a linear correlation is seen. Considering the size
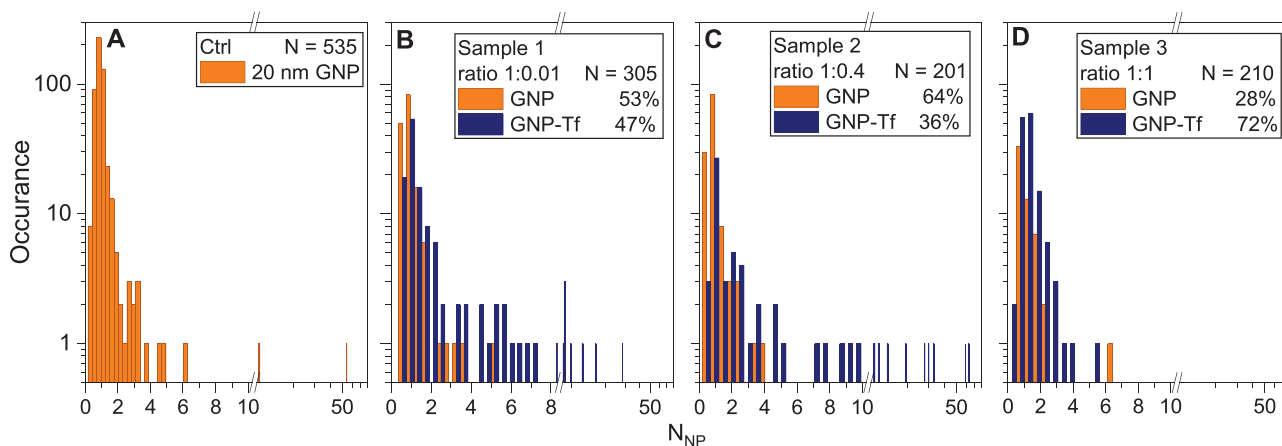
Figure 3. Extinction cross-section of unconjugated GNPs and GNP-Tf constructs. Histogram of N_{NP} measured on unconjugated 20 nm diameter GNPs prior to functionalisation (A) and on GNP-Tf constructs in B) Sample 1, C) Sample 2, and D) Sample 3. For the GNP constructs, the results have been separated into GNPs without (GNP, orange) and with (GNP-Tf, dark blue) fluorescence, based on the correlative fluorescence-exciton image analysis. N_{NP} was determined using single GNP extinction cross-sections $\sigma_{sp} = $ 156 nm^2 in (B), and 566 nm^2 in (A), (C), and (D).

distribution of the GNPs (as shown in Figure 3B), σ_{ext} in the 100–400 nm^2 range indicates single GNPs that appear to have a wide spread of fluorescence rates, suggesting a distribution in the range of 1–10 fluorophores and thus number or Tf attached per single particle (σ_{ext} and fluorescence rates in Figure 4 are additionally shown in units of σ_{sp} and bleaching steps, to indicate the number of GNPs and fluorophores). We note that the variation of the fluorescence rate per fluorophore can be significant, specifically when bound to a GNP, so that the actual distribution of fluorophore number per GNP is likely narrower. With increasing σ_{ext}, indicating GNP multimers in the PSF (likely due to NP cross-linking), the distribution becomes narrower due to averaging of the single particle variabilities across the multimer (ensemble averaging). A different behavior is observed for sample 3 (Figure 4C) where σ_{ext} is relatively constant indicating mostly single particles, again with a wide variability in fluorescence rates (100–2000 pe s^{-1}, indicating 1–15 fluorophores). Hence this sample shows a suppression of GNP cross-linking, but still a high variability in the number of attached fluorophores per particle. Sample 2 shows a behavior (Figure 4B) that is a combination

of what is observed in samples 1 and 3, namely a population of single GNPs conjugated to different numbers of Tf, as well as a linear correlation for cross-linked particles. Figure 4D shows the overall fractions of unconjugated Tf, conjugated GNP-Tf constructs, and unconjugated GNPs in the samples. From this comparison, we observe that increasing the concentration of Tf during reaction steps reduces the presence of unconjugated GNPs. From an application perspective, this is useful since unconjugated GNPs are undesirable in targeted cell uptake experiments as they might contribute to non-specific interactions.[51] On the other hand, considering the high abundance of unconjugated protein especially in sample 3, it is surprising that the fraction of conjugated constructs is not higher. A possible reason for this may be hydrolysis of the sulfo-SMCC crosslinking agent which is known to hydrolyze quickly in aqueous solutions. This can be reduced by performing the reaction at low temperatures.[52] Possibly, hydrolysis occurred before unconjugated particles encountered a reaction partner. As already mentioned, another reason for the large fraction of unconjugated protein might be the tendency of proteins to form a soft corona around NPs[49,53] that is
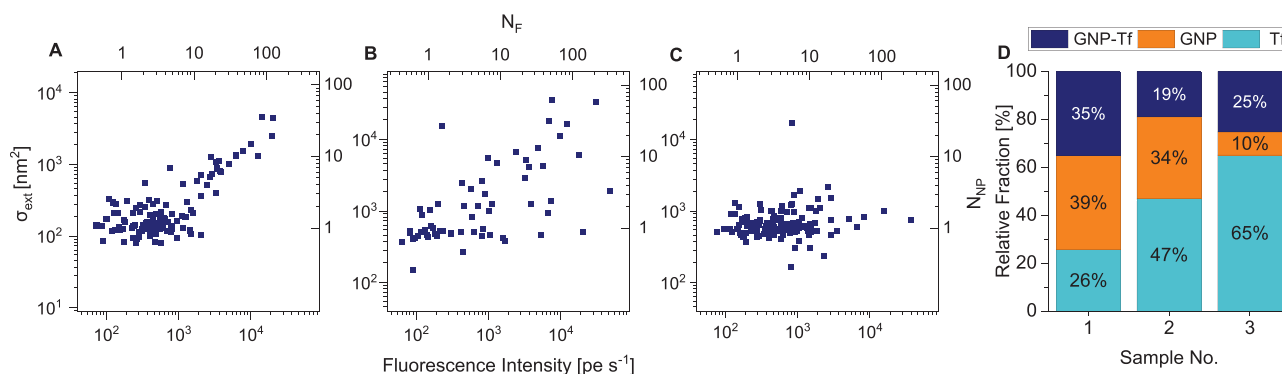

Figure 4. Characteristics of construct samples. Correlation of extinction cross-section and fluorescence rates for GNP-Tf constructs from A) Sample 1, B) Sample 2, and C) Sample 3. Larger extinction cross-sections indicate a higher number of cross-linked particles while higher fluorescence rates indicate a higher number of bound Tf. D) Fractions of unbound protein (light blue), unconjugated particles (orange), and successfully Tf-conjugated GNPs (dark blue) of each sample.

**ADVANCED
SCIENCE NEWS**

www.advancedsciencenews.com

**ADVANCED
MATERIALS
INTERFACES**

www.advmatinterfaces.de

then separated from the construct during spin coating. Furthermore, there might be a risk of trapping proteins between NPs during centrifugation. It is nevertheless clear that sample purification which enables a pure, stable population of functionalized NPs must be optimized before cell internalization studies are performed. The cross-correlation analysis developed here presents an opportunity to assess purification strategy success across conjugated samples before their use.

4. Conclusion

We have developed a novel strategy for the quantitative analysis of the functionalization of GNPs decorated with fluorescently labeled proteins on a particle-by-particle basis, by means of optical microscopy on GNP-protein constructs sparsely deposited onto a glass surface. The number of proteins per particle is assessed using widefield fluorescence microscopy combined with an analysis of the fluorescence bleaching step from a single fluorophore, which enables to quantify the number of fluorophores per single protein, and in turn the number of proteins per single particle. The presence, size, and number of GNPs are quantitatively characterized using extinction microscopy. The cross-correlative analysis of fluorescence and extinction microscopy gives a quantitative measure of the fraction of single GNPs conjugated to fluorescent proteins, versus unconjugated proteins and GNPs, and the formation of GNP multimers suggesting cross-linked particles. From our results, we were able to identify which steps of the conjugation reaction need further improvement. Albeit demonstrated here with spherical GNPs and transferrin proteins, our technique is widely applicable to plasmonic nanostructures of various shapes and materials functionalized with fluorescent biomolecules. Notably, the method is based on relatively simple and easy-to-use widefield microscopy instrumentation, lending itself for widespread adoption of the technique to improve the characterization of nano-formulation systems. The technique can be further simplified by combining fluorophore photobleaching and extinction microscopy on the same imaging system, removing the need for post-acquisition alignment.

Supporting Information

Supporting Information is available from the Wiley Online Library or from the author.

Acknowledgements

Conflict of Interest

The authors declare no conflict of interest.

Author Contributions

Data Availability Statement

Keywords

[1] X. Liu, M.-H. Liu, Y.-C. Luo, C.-Y. Mou, S. D. Lin, H. Cheng, J.-M. Chen, J.-F. Lee, T.-S. Lin, *J. Am. Chem. Soc.* **2012**, *134*, 10251.
[2] H. Xin, L. Lin, R. Li, D. Li, T. Song, R. Mu, Q. Fu, X. Bao, *J. Am. Chem. Soc.* **2022**, *144*, 4874.
[3] S. Lin, Q. Wang, M. Li, Z. Hao, Y. Pan, X. Han, X. Chang, S. Huang, Z. Li, X. Ma, *ACS Catal.* **2022**, *12*, 3346.
[4] Z. You, Q. Qiu, H. Chen, Y. Feng, X. Wang, Y. Wang, Y. Ying, *Biosens. Bioelectron.* **2020**, *150*, 111896.
[5] S. A. Hashemi, S. M. Mousavi, S. Bahrani, S. Ramakrishna, A. Babapoor, W.-H. Chiang, *Anal. Chim. Acta* **2020**, *1107*, 183.
[6] D. M. Fernandes, M. Costa, C. Pereira, B. Bachiller-Baeza, I. Rodríguez-Ramos, A. Guerrero-Ruiz, C. Freire, *J. Colloid Interface Sci.* **2014**, *432*, 207.
[7] A. R. Shahverdi, A. Fakhimi, H. R. Shahverdi, S. Minaian, *Nanomed.: Nanotechnol. Biol. Med.* **2007**, *3*, 168.
[8] J. M. Stern, V. V. Kibanov Solomonov, E. Sazykina, J. A. Schwartz, S. C. Gad, G. P. Goodrich, *Int. J. Toxicol.* **2016**, *35*, 38.
[9] M. A. Garcia, *J. Phys. D: Appl. Phys.* **2012**, *45*, 389501.
[10] I. Pope, H. Tanner, F. Masia, et al., *Light Sci. Appl.* **2023**, *12*, 80.
[11] I. Pope, N. G. C. Ferreira, P. Kille, W. Langbein, P. Borri, *Appl. Phys. Lett.* **2023**, *122*, 153701.
[12] B. Van Den Broek, B. Ashcroft, T. H. Oosterkamp, J. Van Noort, *Nano Lett.* **2013**, *13*, 980.
[13] K. Chen, Y. Gu, W. Sun, Bin Dong, G. Wang, X. Fan, T. Xia, N. Fang, *Nat. Commun.* **2017**, *8*, 887.
[14] K. L. Kelly, E. Coronado, L. L. Zhao, G. C. Schatz, *J. Phys. Chem. B* **2003**, *107*, 668.
[15] K.-S. Lee, M. A. El-Sayed, *J. Phys. Chem. B* **2006**, *110*, 19220.
[16] B. D. Chithrani, A. A. Ghazani, W. C. W. Chan, *Nano Lett.* **2006**, *6*, 662.
[17] Arnida, M. M. Janát-Amsbury, A. Ray, C. M. Peterson, H. Ghandehari, *Eur. J. Pharm. Biopharm.* **2011**, *77*, 417.
[18] A. Janz, A. Köckritz, L. Yao, A. Martin, *Langmuir* **2010**, *26*, 6783.
[19] M. Clément, H. Ménard, P. A. Rowntree, *Langmuir* **2008**, *24*, 8045.
[20] A. E. James, J. D. Driskell, *Analyst* **2013**, *138*, 1212.
[21] T. Zheng, S. Bott, Q. Huo, *ACS Appl. Mater. Interfaces* **2016**, *8*, 21585.

**ADVANCED
SCIENCE NEWS**

www.advancedsciencenews.com

**ADVANCED
MATERIALS
INTERFACES**

www.advmatinterfaces.de

[22] Y. Yang, S. Liao, Z. Luo, R. Qi, N. Mac Fhionnlaoich, F. Stellacci, S. Guldin, *Nanoscale* **2020**, *12*, 12007.

[23] M. M. Modena, B. Rühle, T. P. Burg, S. Wuttke, *Adv. Mater.* **2019**, *31*, 1901556.

[24] C. Gentilini, F. Evangelista, P. Rudolf, P. Franchi, M. Lucarini, L. Pasquato, *J. Am. Chem. Soc.* **2008**, *130*, 15678.

[25] K. B. Sebby, E. Mansfield, *Anal. Bioanal. Chem.* **2015**, *407*, 2913.

[26] S. Elzey, D.-H. Tsai, S. A. Rabb, L. L. Yu, M. R. Winchester, V. A. Hackley, *Anal. Bioanal. Chem.* **2012**, *403*, 145.

[27] S. J. Hurst, A. K. R. Lytton-Jean, C. A. Mirkin, *Anal. Chem.* **2006**, *78*, 8313.

[28] H. D. Hill, J. E. Millstone, M. J. Banholzer, C. A. Mirkin, *ACS Nano* **2009**, *3*, 418.

[29] A. M. Smith, L. E. Marbella, K. A. Johnston, M. J. Hartmann, S. E. Crawford, L. M. Kozycz, D. S. Seferos, J. E. Millstone, *Anal. Chem.* **2015**, *87*, 2771.

[30] D. Zhang, S. M. Ansar, *Anal. Chem.* **2010**, *82*, 5910.

[31] L. Mohrhusen, M. Osmic, *RSC Adv.* **2017**, *7*, 12897.

[32] N. Giannakopoulou, J. B. Williams, P. R. Moody, E. J. Sayers, J. P. Magnusson, I. Pope, L. Payne, C. Alexander, A. T. Jones, W. Langbein, P. Watson, P. Borri, *Nanoscale* **2020**, *12*, 4622.

[33] B. T. Miles, A. B. Greenwood, D. Benito-Alifonso, H. Tanner, M. C. Galan, P. Verkade, H. Gersen, *Sci. Rep.* **2017**, *7*, 44666.

[34] R. Lévy, U. Shaheen, Y. Cesbron, V. Sée, *Nano Rev.* **2010**, *1*, 4889.

[35] A. M. Smith, K. A. Johnston, S. E. Crawford, L. E. Marbella, J. E. Millstone, *Analyst* **2017**, *142*, 11.

[36] L. M. Payne, W. Albrecht, W. Langbein, P. Borri, *Nanoscale* **2020**, *12*, 16215.

[37] L. M. Payne, W. Langbein, P. Borri, *Appl. Phys. Lett.* **2013**, *102*, 131107.

[38] L. M. Payne, Extinction Suite Macro, http://langsrv.astro.cf.ac.uk/Crosssection/Crosssection.html (accessed: December 2021).

[39] P. B. Johnson, R. W. Christy, *Phys. Rev. B* **1972**, *6*, 4370.

[40] L. M. Payne, F. Masia, A. Zilli, W. Albrecht, P. Borri, W. Langbein, *J. Chem. Phys.* **2021**, *154*, 044702.

[41] A. Bumb, S. K. Sarkar, X. S. Wu, M. W. Brechbiel, K. C. Neuman, *Biomed. Opt. Express* **2011**, *2*, 2761.

[42] J. R. Lakowicz, Y. Fu, *Laser Photonics Rev.* **2009**, *3*, 221.

[43] G. P. Acuna, M. Bucher, I. H. Stein, C. Steinhauer, A. Kuzyk, P. Holzmeister, R. Schreiber, A. Moroz, F. D. Stefani, T. Liedl, F. C. Simmel, P. Tinnefeld, *ACS Nano* **2012**, *6*, 3189.

[44] T. L. Doane, Y. Cheng, A. Babar, R. J. Hill, C. Burda, *J. Am. Chem. Soc.* **2010**, *132*, 15624.

[45] H. Liu, T. L. Doane, Y. Cheng, F. Lu, S. Srinivasan, J.-J. Zhu, C. Burda, *Part. Part. Syst. Charact.* **2015**, *32*, 197.

[46] C. A. Enns, H. H. Sussman, *J. Biol. Chem.* **1981**, *256*, 9820..

[47] G. T. Hermanson, *Bioconjugate Techniques*, Academic Press, Cambridge, Massachusetts **2013**.

[48] D. Bonvin, D. Chiappe, M. Moniatte, H. Hofmann, M. Mionic Ebersold, *Analyst* **2017**, *142*, 3805.

[49] H. Mohammad-Beigi, Y. Hayashi, C. M. Zeuthen, H. Eskandari, C. Scavenius, K. Juul-Madsen, T. Vorup-Jensen, J. J. Enghild, D. S. Sutherland, *Nat. Commun.* **2020**, *11*, 4535.

[50] S. J. Park, *Int. J. Nanomedicine* **2020**, *15*, 5783.

[51] E. Oh, J. B. Delehanty, K. E. Sapsford, K. Susumu, R. Goswami, J. B. Blanco-Canosa, P. E. Dawson, J. Granek, M. Shoff, Q. Zhang, P. L. Goering, A. Huston, I. L. Medintz, *ACS Nano* **2011**, *5*, 6434.

[52] M. Pereira, E. P. Lai, *J. Nanobiotechnol.* **2008**, *6*, 10.

[53] T. Cedervall, I. Lynch, S. Lindman, T. Berggård, E. Thulin, H. Nilsson, K. A. Dawson, S. Linse, *Proc. Natl. Acad. Sci. USA* **2007**, *104*, 2050.

2300568 (9 of 9)